Design of Noncontact Lap Splice Connections for C-PSW/CF (SpeedCore)

SHIVAM SHARMA, SOHEIL SHAFAEI, AMIT VARMA, and RON KLEMENCIC

ABSTRACT

Concrete-filled composite plate shear walls (C-PSW/CF) are an emerging structural system in building construction. The composite wall-to-base connection is a critical component influencing system behavior and design. Different types of composite wall-to-base connections are possible, but the noncontact lap splice connection between the dowel bars of the reinforced concrete (RC) base and the steel faceplates of the composite walls is of interest due to its constructability and potential structural efficiency. This type of wall-to-base connection can govern the lateral resistance of the overall wall system, which may be acceptable for wind loading situations and, depending on ductility, may also be acceptable for seismic loading conditions. This study presents the design and detailing of noncontact dowel bar lap splice connections for composite walls-to-RC foundations or walls. Design parameters include embedment length and arrangement of dowel bars within the composite wall cross section and the interfacial shear strength provided using ties or a combination of ties and stud anchors (shear studs) to transfer forces from the dowel bar to the steel faceplates. Previous recommendations for these parameters, provided in the literature, are used and verified experimentally. Three large-scale specimens with different connection details are designed, constructed, and tested to failure. The experimental results are evaluated, and design recommendations are proposed along with methods to calculate the flexural stiffness and flexural strength of the composite wall-to-base connections.

Keywords: composite plate shear walls/concrete-filled, SpeedCore system, experimental study, seismic and wind design, lap splice, connections, composite walls, wall-to-foundation connection.

INTRODUCTION

Concrete-filled composite plate shear walls (C-PSW/CF) effectively combine the advantages of steel construction with concrete materials to result in a composite wall system that has excellent structural performance and efficient constructability. These composite plate shear walls have been used in the construction of nuclear power plants (e.g., AP 1000®) and energy related structures, where they are referred as steel-plate composite (SC) structures and designed in accordance with the ANSI/AISC N690, *Specification for Safety-Related Steel Structures for Nuclear Facilities* (AISC, 2024), hereafter referred to as AISC N690–24, and AISC Design Guide 32, *Modular Steel-Plate Composite Walls for Safety-Related Nuclear Facilities* (Bhardwaj and Varma, 2017).

The use of composite plate shear walls has gained more acceptance in the commercial building construction industry over the past few years due to the advantages of modularization and resulting improvements in construction schedule. For example, the construction of Rainier Square Tower (Traut-Todaro, 2019) using C-PSW/CF core walls reduced the construction time by approximately 40% viz-a-viz traditional reinforced concrete (RC) core walls and demonstrated these benefits. The construction of 200 Park Avenue using C-PSW/CF core walls saved 3 months on the overall construction schedule and reduced costs (Klemencic et al., 2023). The system was conferred the name "SpeedCore" by the American Institute of Steel Construction (AISC) in recognition of these advantages.

For example, a planar C-PSW/CF comprised of web and flange steel plates, forming a box section enclosing the concrete infill, is shown in Figure 1. Complete-joint-penetration (CJP) groove welds are typically used to connect the flange plates to the web plates. Regularly spaced tie bars are used to connect the web plates. They ensure stability of the empty steel modules during the transportation and erection phases. These tie bars can either be welded to the web plates, or threaded rods can also be used. Steel headed stud anchors (also referred to as shear studs) can be used to supplement or partially replace tie bars, offering similar composite action between steel and concrete. These shear studs can be welded to the inner surface of web plates

Shivam Sharma, PhD Candidate, Lyles School of Civil and Construction Engineering, Purdue University, West Lafayette, Ind. Email: sharm368@purdue.edu (corresponding author)

Soheil Shafaei, PhD, M.ASCE, Assistant Professor, Department of Civil and Environmental Engineering, Utah State University, Logan, Utah. Email: soheil.shafaei@usu.edu

Amit Varma, PhD, M.ASCE, Karl H. Kettelhut Professor, Lyles School of Civil and Construction Engineering, Purdue University, West Lafayette, Ind. Email: ahvarma@purdue.edu

Ron Klemencic, PE, SE, Dist.M.ASCE, President and CEO, Magnusson Klemencic Associates (MKA), Seattle, Wash. Email: rklemencic@mka.com

Paper No. 2024-15

(Bhardwaj et al., 2017). In C-PSW/CF, steel plates provide the primary resistance to tensile and shear stresses, whereas the concrete infill contributed to resisting compressive and shear stresses while acting composite with the steel. Acting together through composite action, both steel and concrete enhance the flexural and shear stiffness of the system.

A C-PSW/CF system could either be coupled or uncoupled. ASCE 7-16 (2016) included uncoupled C-PSW/CF as a seismic force-resisting system, and the corresponding design provisions were first laid out in the 2016 ANSI/AISC *Seismic Provisions for Structural Steel Buildings* (AISC, 2016) and further enhanced in the 2022 version of the AISC *Seismic Provisions for Structural Steel Buildings* (AISC, 2022a), hereafter referred to as the AISC *Seismic Provisions*, and in the 2022 version of the AISC *Specification for Structural Steel Buildings* (AISC, 2022b), hereafter referred to as the AISC *Specification*, based on recent research (Agrawal et al., 2020; Broberg et al., 2023).

In design situations with high base shear and overturning moments (e.g., taller buildings), it is beneficial to connect the individual (or uncoupled) C-PSW/CF to each other using coupling beams, resulting in coupled C-PSW/CF system. ASCE 7–22 (2022) incorporated seismic modification factors for coupled C-PSW/CF, and the design and detailing requirements were included in the 2022 AISC *Seismic Provisions* and in the 2022 AISC *Specification* based on recent research (Broberg et al., 2022; Kizilarslan et al., 2021; Ahmad et al., 2024).

PRIOR INVESTIGATIONS

The response of C-PSW/CF under wind and seismic loading has been studied extensively. Design recommendations based on experimental and numerical studies (Shafaei et al., 2022, 2023) have been outlined and incorporated into AISC Design Guide 38, *SpeedCore Systems for Steel Structures* (Varma et al., 2023).

The lateral forces resisted by these walls and the corresponding base shear and overturning moment need to be transferred to the base, making this connection a critical aspect in their commercial applications. C-PSW/CF may be connected directly to the RC foundation or through an RC wall. The C-PSW/CF–RC wall connection may be favored for certain projects due to lower costs of construction and other design preferences. In both cases, the embedded dowel bar technique, commonly referred as a noncontact lap splice connection, can be effective in establishing the connection between the C-PSW/CF and the RC base, with or without an RC wall. In this type of connection, the forces from the C-PSW/CF steel plates are transferred to the dowels through the formation of compression struts in the concrete infill. For example, Figure 2 illustrates the force transfer from C-PSW/CF flange plate to an adjacent dowel bar. The tensile stresses in the dowels are transferred to the surrounding concrete through the concrete-dowel rebar bond.

Seo and Varma (2017) conducted experimental and numerical investigations on the behavior of SC-to-RC

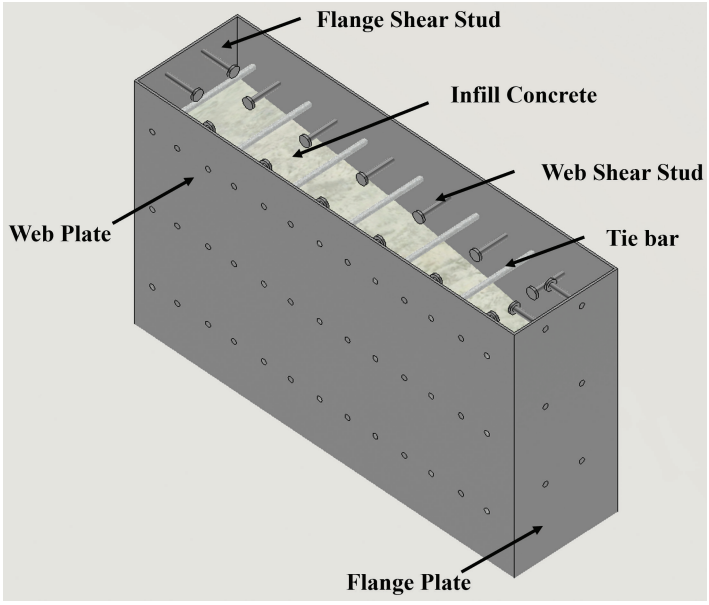

Fig. 1. Typical details of planar (uncoupled) C-PSW/CF.

noncontact lap splice connections and developed recommendations for their design and detailing. These included (1) using continuous tie bars in the SC walls to prevent splitting failure, (2) providing adequate embedment/development length for the dowel bars in both the C-PSW/CF and RC base, (3) providing sufficient shear studs/tie bars for interfacial shear transfer, and (4) placing the dowel at a minimum distance from the steel faceplates for complete formation of compression struts. Seo et al. (2021) corroborated and expanded these recommendations by conducting further experiments. They suggested using a maximum distance between steel faceplates and dowel rebar for ductile failure.

Cyclic tests on SC wall-to-RC foundation lap splice connections were conducted by Wang et al. (2020) to evaluate their seismic performance. The connections exhibited highly ductile behavior and failed in a flexure-dominated mode, marked by tensile yielding of the dowels. Kurt et al. (2022) investigated the behavior of lap splice connections under cyclic lateral load. The development length of dowels in the connection was in accordance with ACI 318-19 (2019), and they were expected to reach their yield strength. The connections exhibited highly ductile behavior with failure occurring due to crushing of concrete in compression followed by tensile rupture of the dowels. Both these studies demonstrate that the noncontact lap splice technique is an effective way of connecting C-PSW/CF to the RC foundation. Moreover, unlike these studies where infill concrete spalling led to lower connection capacity, the presence of flange plates required in C-PSW/CF as per the AISC *Specification* will constrain the concrete from spalling, thus providing additional confinement of the dowels. Consequently, the dowels are expected to achieve their ultimate tensile strength, thus enhancing the overall ductility of the connection. Additionally, evaluating the performance of these connections for wind loading histories can provide valuable insights while designing for wind-governed designs.

This paper presents the design and detailing of noncontact lap splice connections for C-PSW/CF for wind and seismic applications. Three full-scale specimens—including two specimens connecting C-PSW/CF to the RC foundation and one connecting C-PSW/CF to the RC wall with different connection details—are designed and experimentally evaluated. Design recommendations for prescriptive design of noncontact lap splice connections for C-PSW/CF are provided for engineers. In addition, methods to calculate the flexural stiffness and flexural capacities of the connections are proposed.

DESIGN OF NONCONTACT LAP SPLICE CONNECTIONS

Wind and seismic events impose large force demands on noncontact splice connections. The tensile stresses from steel plates of C-PSW/CF must be transferred to the dowels continuing into the RC base. To ensure adequate strength, ductility, and energy dissipation during such events, the design of these connections should favor limit states like yielding of the dowel bar or C-PSW/CF steel plates while avoiding premature failure in the stud anchors, dowel bar pullout, or concrete infill splitting.

The overall system consists of (1) the C-PSW/CF wall; (2) the RC base—that is, wall and/or foundation; and (3) the noncontact lap splice connection region between the wall and the base. This section discusses the design and detailing recommendations available in literature for developing ductile failure modes that consist of yielding in the dowel

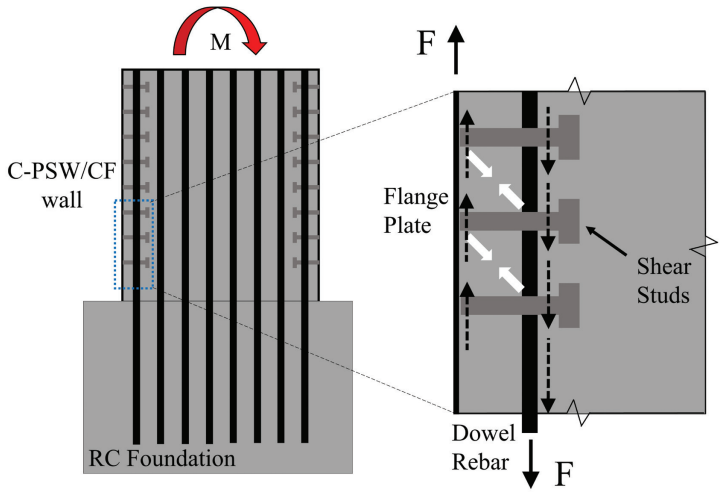

Fig. 2. Load transfer mechanism in the noncontact lap splice connection.

bars of the connection region. For further clarity, the RC section in the connection region, which is confined by the steel modules of C-PSW/CF, is referred to as the "confined RC section."

Confined RC Section

AISC *Seismic Provisions* Section H7.7c specifies that the C-PSW/CF-to-foundation connection should be detailed such that the connection is able to transfer the base shear force, axial force, and overturning moment corresponding to 1.1 times the plastic flexural strength of the composite wall. This is comparable to the full-strength design philosophy specified in AISC N690-24, which requires the connection to develop at least 125% of the nominal strength of the weaker of the two connected components.

The noncontact lap splice connection can be designed to develop the full strength of the composite wall. However, it is typically designed and detailed to develop the full strength of the confined RC section in the connection region, which will be the weaker of the two connected components. This is done to improve constructability by reducing rebar congestion. This is also practical for wind-governed designs where the connection must be designed only for the calculated demands. This may also be practical for situations where the steel plates of the C-PSW/CF are overdesigned (in terms of plate thickness) to facilitate fabrication, handling, etc., and/or to meet drift requirements if they govern over strength requirements.

The contributions of the C-PSW/CF steel plates are not considered while calculating the strength (e.g., axial, flexural, etc.) of the confined RC section. Analytical methods have been developed by the authors to calculate the flexural and shear capacities of the confined RC section. These methods have been adapted from existing design codes and are presented later in this paper.

Design Recommendations

The recommendations provided by Seo and Varma (2017) and Seo et al. (2021) were used to design and detail the connection region. While the presence of steel flange plates and tie bars in C-PSW/CF helps in inhibiting splitting failure, requirements concerning interfacial shear, dowel bar development length, and appropriate placement of dowel bars still need to be met.

Interfacial Shear Strength

The connection must be designed to have interfacial shear strength greater than or equal to 1.25 times the nominal yield strength of the dowel bars in the confined RC section. The connection interfacial strength is the sum of the nominal shear strength provided by tie bars and shear studs inside the dowel embedment region. Direct shear strength equations provided in AISC *Specification* Section I8.3a, are used for the shear studs, and those developed by Seo et al. (2019) are adapted for the threaded tie rods. These equations are presented later in the paper.

Embedment/Development Length

Wall Portion

Adequate embedment length needs to be provided for the dowels to develop their full tensile strength. Development lengths for deformed bars can be calculated using ACI 318-19, Section 25.4.2.3 or 25.4.2.4. The shorter development lengths calculated using ACI 318-19, Section 25.4.2.4, account for the effects of confinement. For tension splice lengths, ACI 318-19, Section 25.5.2, recommends using a multiplication factor of 1.3. However, multiplying the development lengths calculated using ACI 318-19, Section 25.4.2.3 (which does not account for effects of confinement), by 1.3 can lead to extremely conservative designs. Therefore, the development lengths calculated using ACI 318-19, Section 25.4.2.4 (which includes the effects of confinement), multiplied by the factor of 1.3 are recommended as the minimum embedment length for design and detailing.

RC Base Portion

The development length for hooked dowel bars in the RC base can be calculated using ACI 318-19, Section 25.4.3.1. These hooked dowel bars need to be provided with the minimum inside bend diameter and straight extension length in accordance with ACI 318-19, Table 25.3.1. However, in most practical cases, these bars are just extended to the bottom of the RC base for convenience.

Dowel Location

To facilitate the development of concrete compression struts between C-PSW/CF steel plates and the dowel bars, the spacing between the dowels and the interior surface of C-PSW/CF steel plates must be greater than the diameter of the dowel. At the same time, the dowel in the exterior layers must also be placed within the length of shear stud anchors and those in the middle layers must be placed within the length of the tie bars, as shown in Figure 3. These recommendations follow those by Seo and Varma (2017) and Seo et al. (2021).

EXPERIMENTAL PROGRAM AND RESULTS

Three specimens with noncontact lap splice connections were tested under wind and seismic loading and their behavior was evaluated. Two of these specimens (SP-1 and SP-2)

consisted of C-PSW/CF wall connected to RC foundation directly, while one (SP-3) included an RC wall in-between. Figure 3 shows these two types of connections evaluated in this study.

As shown in Figure 3, the dowel bars form a noncontact lap splice with the steel plates of C-PSW/CF and facilitate the transfer of tensile forces from C-PSW/CF to the RC foundation. The connection region consists of an RC section with rebar dowels embedded in the C-PSW/CF, previously defined as the confined RC section. Adequate C-PSW/CF wall and foundation embedment lengths, denoted as l_{d_wall} and l_{d_fnd}, respectively, are provided for the dowels to develop the full strength of the confined RC section. Shear studs and tie bars are provided to ensure adequate interfacial strength in the connection. The tie bars also help in preventing splitting failure in the connection. For the connection having an RC wall, transverse shear reinforcement is provided to prevent failure in the RC wall.

Test Matrix

All specimens had an identical C-PSW/CF wall with details provided in Table 1. The C-PSW/CF had length, l_w, and thickness, t_{sc}, of 37.5 in. and 10 in., respectively. ASTM A572/A572M Gr. 50 steel faceplates (ASTM, 2021), having thickness, t_p, of 3⁄16 in., were used in the web whereas the C-shape section, MC 10×8.4, was used as the flange section. ASTM A193 B7 steel threaded tie bars and shear studs (ASTM, 2023) having a diameter of 0.5 in. and spacing of 5 in. on center were provided in the web and flange plates. Figure 4 provides the geometric details of the C-PSW/CF.

For SP-3, the RC wall had a length and thickness of 39.5 in. and 12 in., respectively. The height of the wall was 24 in., extending from the top of the RC foundation to the C-PSW/CF base. It was transversely reinforced using #3 Gr. 60 ties. Several layers of transverse reinforcement were provided to ensure sufficient shear strength, as shown in Figure 4(f). Perimeter hoops with supplemental 135° cross ties were also provided for further reinforcement. The various sublayers of the horizontal reinforcement are shown later in Figure 6.

The connection consisted of dowel bars of different diameters, d_{bar}, and nominal yield strengths, F_{y_bar}. Their details are presented in Table 2. SP-1 and SP-3 consisted of #6 Gr. 60 dowel bars, whereas SP-2 had #8 Gr. 80 dowel bars. These dowels had different embedment lengths in the wall, $l_{d\_wall\_provided}$, as shown in Table 2. For adequate interfacial strength, the dowel embedment region was reinforced with additional shear studs welded to the C-PSW/CF web plate.

The RC foundation block for the specimen was designed to resist all loads originating during the test. SP-1 and SP-2 had identical foundation design, while SP-3 had a different foundation design. Figure 5 shows the geometric details and rebar layout for the foundations for all three specimens.

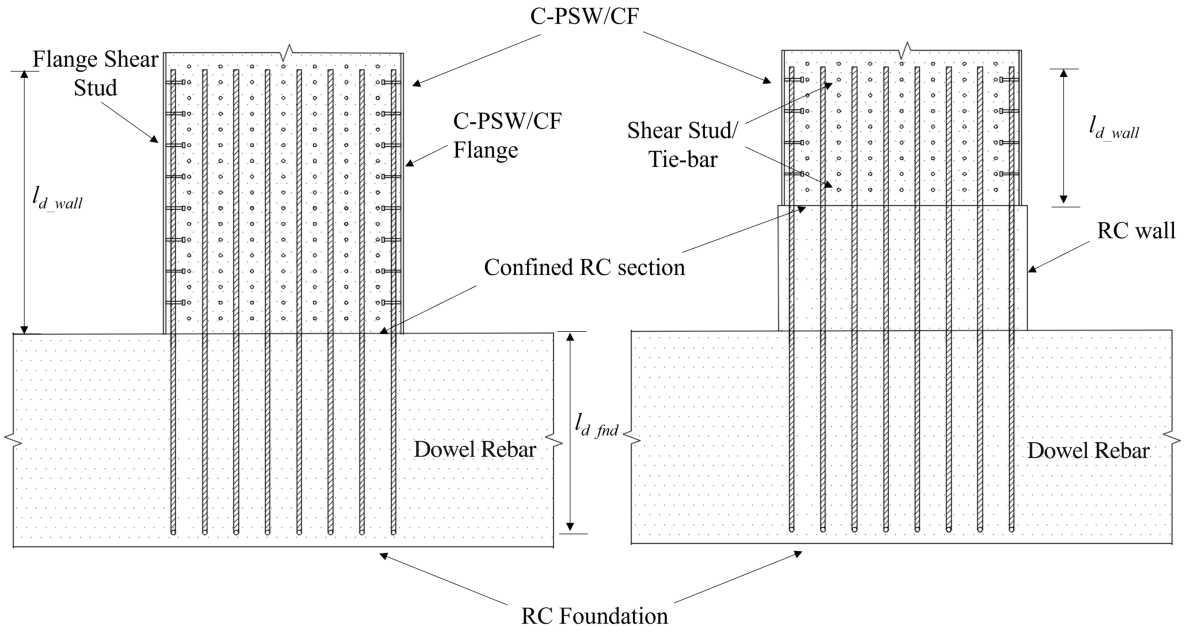

(a) Without RC wall *(b) With RC wall*

Fig. 3. Schematics of the noncontact lap splice connections.

Table 1. Details of Planar C-PSW/CF														
General			Web											Flange
h_w (in.)	l_w (in.)	t_{sc} (in.)	t_p (in.)	ρ %	s_{stud} (in.)	d_{stud} (in.)	F_{u_stud} (ksi)	$\frac{s_{stud}}{t_p}$	s_{tie} (in.)	d_{tie} (in.)	F_{y_tie} (ksi)	$\frac{s_{tie}}{t_p}$	ρ_{tie} %	MC 10×8.4
120	37.5	10	3/16	3.75	5	0.5	65	26.7	5	0.5	60	26.7	0.78	

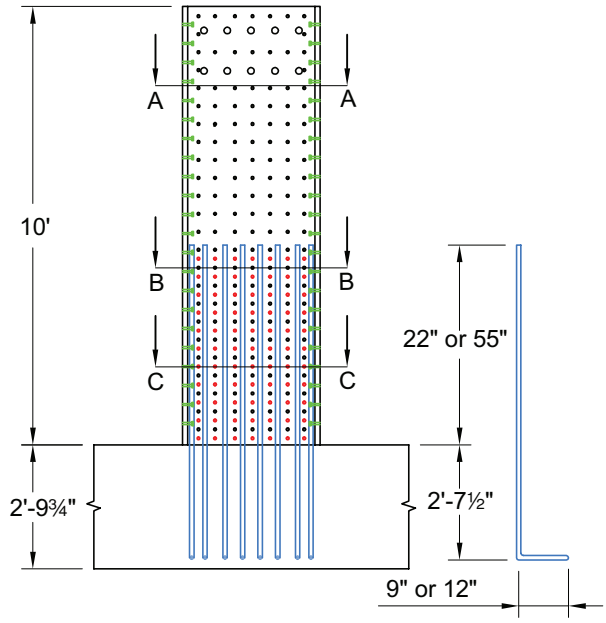

(a) SP-1 and SP-2

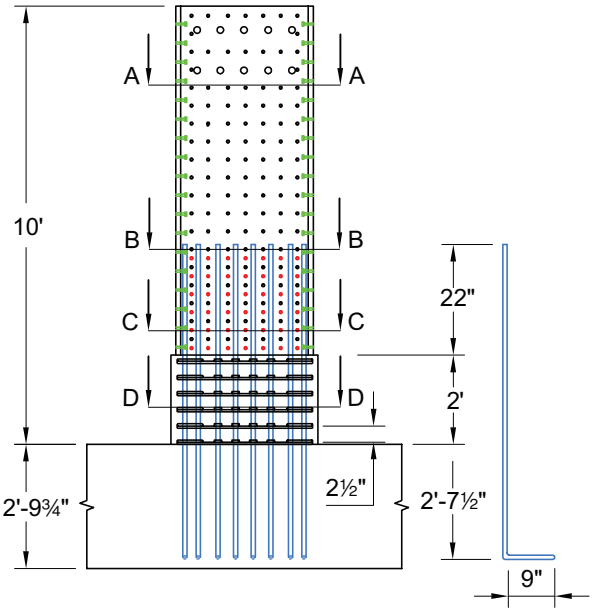

(b) SP-3

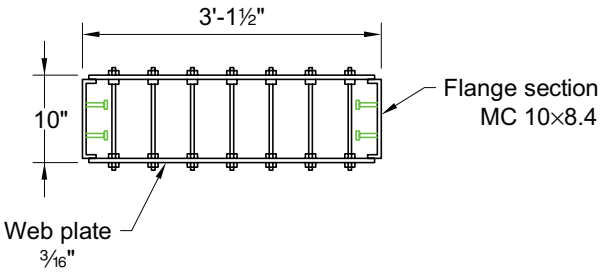

(c) Section A-A

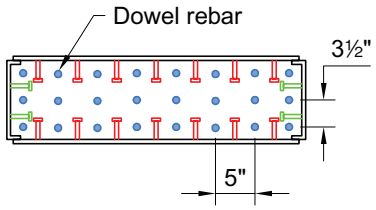

(d) Section C-C

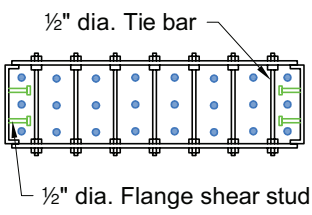

(e) Section B-B

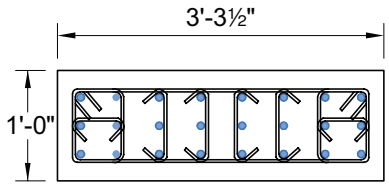

(f) Section D-D

Fig. 4. Specimen geometric details.

Table 2. Details of Dowels in Lap Splice Connections			
	Dowels		
Specimen	F_{y_bar} (ksi)	$l_{d\_wall\_provided}$ (in.)	d_{bar} (in.)
SP-1	60	22	¾
SP-2	80	55	1
SP-3	60	22	¾

Design of Test Specimens

This section presents the design details of the test specimens.

C-PSW/CF Wall Portion

Several archetype structures, using coupled and uncoupled C-PSW/CF systems for the primary lateral-force-resisting system, were designed for wind and seismic loading governed designs (Shafaei et al., 2022). The planar C-PSW/CF wall portions used in the cyclic experiments represented the individual walls of these uncoupled or coupled C-PSW/CF systems subjected to axial forces and lateral loading. The specimens were not precisely scaled down models of the individual planar C-PSW/CF walls of the archetype building structures. Instead, relevant structural characteristics were retained, such as (1) the steel reinforcement ratio ($\rho = 2t_p/t_{sc}$), (2) the steel plate slenderness ratio (s/t_p), (3) the tie bars reinforcement ratio ($\rho_{tie} = 2A_{tie}/s_{tie}$), and (4) the tie

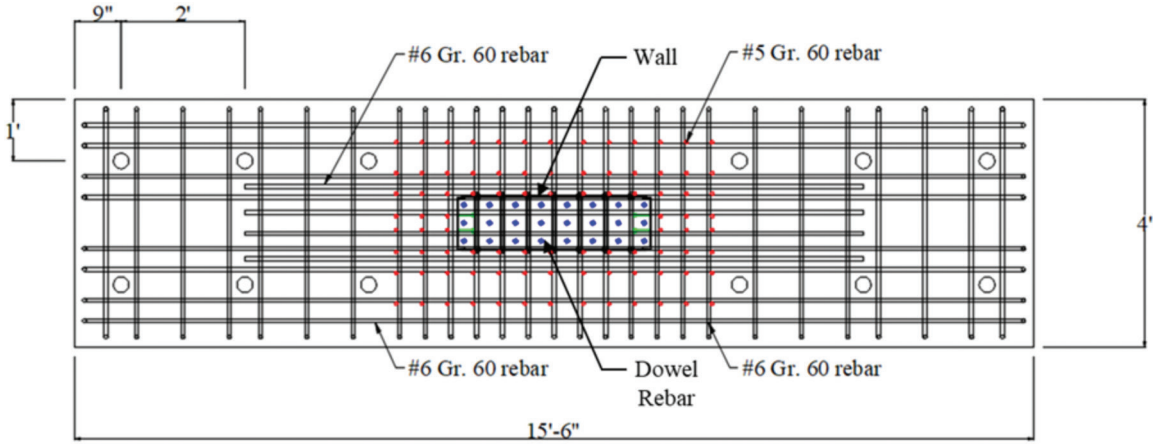

(a) SP-1 and 2

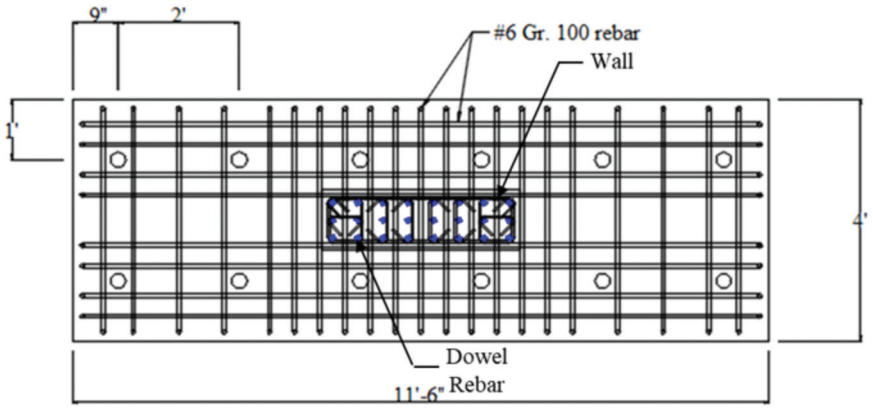

(b) SP-3

Fig. 5. Foundation details.

bar spacing to wall thickness ratio (s_{tie}/t_p). All ratios met the applicable requirements of AISC *Specification* Section I-1.5 and the AISC *Seismic Provisions*. The height-to-length ratio of the wall specimens was close to 3.0 to ensure flexure-dominant behavior. The authors have tested similar C-PSW/CF wall specimens with other types of wall-to-base connections that were designed to develop the full strength (plastic flexural capacity) of the C-PSW/CF walls under wind and seismic loading conditions (Shafaei et al., 2021, 2023).

RC Wall Portion (SP-3 Only)

The RC wall portion was designed using ACI 318-19, Chapter 18, to resist seismic loads while providing ductile inelastic response. For design, the height of the wall, h_w, was taken as 9 ft, which was the distance between the base of the RC and the load application point during the cyclic tests. The wall section was 39.5 in. long and 12 in. wide. Consequently, the coefficient of concrete contribution to wall shear strength, α_c, was taken as 2.0, per ACI 318-19, Section 18.10.4.1.

Dowel bars served as the longitudinal reinforcement for the RC wall. In addition, transverse reinforcement was provided for adequate shear strength. Figure 6 presents the various layers of transverse reinforcements provided in the RC wall. The reinforcement was provided in two orthogonal directions as per ACI 318-19, Section 18.10.4.3. In addition to horizontal web reinforcement, perimeter hoops with supplemental 135° cross ties and through web cross ties were also provided. Here, #3 Gr. 60 steel was used for the transverse reinforcement. The longitudinal and transverse wall reinforcement ratios (ρ_l and ρ_t) were 0.022 and 0.007, respectively, greater than the required value of 0.0025 as per ACI 318-19, Section 18.10.2.1.

The nominal shear strength of the RC wall, V_n, was calculated using the expression provided in ACI 318-19, Section 18.10.4.1, subject to an upper limit (shear strength of $10\sqrt{f'_c}A_{cv}$, where f'_c is expressed in psi and A_{cv} is the area of the concrete cross section). The nominal shear strength of the RC wall was calculated as 289 kips, which is approximately 73% of the upper limit. While designing, it was ensured that the RC wall had adequate shear strength, V_n, to transfer the lateral force, H_n, corresponding to the flexural strength of the confined RC section in the connection region, which was calculated as 142 kips (explained later).

Table 3 summarizes the geometric properties and design strengths for the RC wall.

Noncontact Lap Splice Connection Region

The full-strength connection design philosophy and the design recommendations discussed earlier were used to design and detail the noncontact lap splice connections. The applied loading subjects the connection region to axial force, *P,* bending moment, *M*, and shear force, *V*. The *P-M* combination results in tensile stresses (and forces) in the dowel bars on the tension side of the neutral axis. Under reversed cyclic loading, the dowel bars at both ends of the section are subjected to large tensile stresses and strains. The shear force, *V*, is resisted by either a direct shear mechanism or shear friction mechanism afforded by the dowel bars closer to the center (neutral axis) of the cross section. Thus, all the dowel bars in the connection region are subjected to large tensile stresses. Consequently, the design and detailing of dowel bars in the connection region focuses on developing their tensile strength.

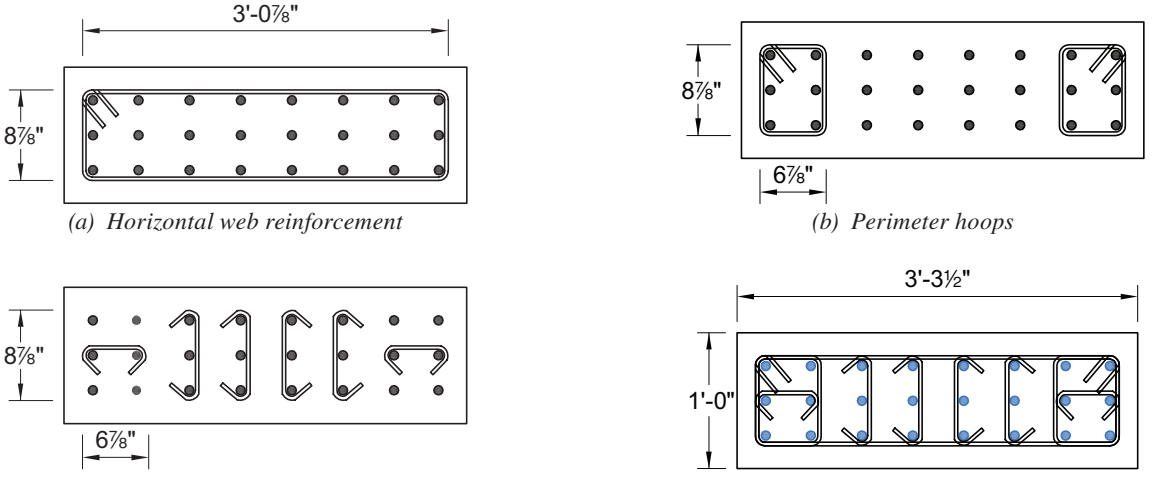

(a) Horizontal web reinforcement

(b) Perimeter hoops

(c) Cross ties

(d) All shear reinforcement (Section D-D in Figure 4)

Fig. 6. RC wall cross section.

Table 3. Section Details and Calculations for the RC Wall	
RC Wall Dimensions	
h_w, ft	9.0
l_w, in.	39.5
t_w, in.	12.0
Design Parameters	
h_w/l_w	2.83
α_c	2.00
Wall Reinforcement	
ρ_l	0.022
ρ_t	0.007
ρ_{min_req}	0.0025
Shear Strength	
V_n, kips (ACI 318, Section 18.10.4.1)	289
$\frac{V_n}{10\sqrt{f'_c}A_{cv}}$	0.727
H_n, kips	142

The connections were designed to develop the full tensile strength, N_r, of the weaker of the connected parts—that is, 1.25 times the nominal yield strength of the dowels $A_{bar}F_{y\_bar}$ in the connection. The tensile forces in the dowels are transferred to the steel plates of the C-PSW/CF by interfacial shear stresses produced by direct shear of the stud anchors and tie bars (see Figure 2). The connections were detailed such that the net interfacial strength, $\sum_n Q_n$, calculated as the sum of the direct shear strengths of the stud anchors (ψR_{stud}) and tie bars (ψR_{tie}) in the dowel embedment region, exceeded the required tensile strength (N_r) to be transferred through them. In the specimens, the direct shear strengths of individual headed stud anchors and threaded rods were calculated using Equation 1 from AISC *Specification* Section I8.3a, and Equation 2 adapted from Seo et al. (2019), respectively. In Equation 1, A_{stud} and F_{u_stud} denote the gross cross-sectional area and nominal tensile strength of the stud anchors, respectively. In Equation 2, A_{tie} and F_{y_tie} denote the gross cross-sectional area and nominal yield strength of the threaded rods, respectively. The 0.75 factor accounts for the effects of threads on the cross-sectional area, and 0.577 relates the tensile yield to shear yield stress.

$$\phi R_{stud} = (0.65)(1.0)A_{stud}F_{u\_stud} \quad (1)$$

$$\phi R_{tie} = (0.577)(0.75)A_{tie}F_{y\_tie} \quad (2)$$

Minimum spacing limits of the dowels were checked in accordance with ACI 318-19, Section 25.2. The minimum spacing of the dowels was taken as the greater of (1) 1 in., (2) the dowel bar diameter, or (3) 4/3 times the maximum size of aggregate. For effective development of concrete compression struts, the exterior layers of dowel bars were included within the length of the stud anchors, and the middle layer was included within the length of the tie bars.

The development length for dowel bars in the wall was calculated using ACI 318-19, Section 25.4.2.4, and then multiplied with 1.3 in accordance with Section 25.5.2 to calculate the required embedment length, l_{d_wall}. Hooked dowel bars were used in the foundation with development lengths also calculated using ACI 318-19. The calculated and provided values for the development lengths are listed in Table 4.

Test Setup and Loading Protocol

The test setup used for cyclic testing was similar to that used by Shafaei et al. (2021, 2023). Lateral and axial loads were applied to the top of the specimen after fixing them to the strong floor using 1¾-in.-diameter post-tensioning rods. Axial force, corresponding to 10% of the axial compression strength of the confined RC section, was applied at the top of the specimen. The axial loading was applied using a 500 ton Enerpac ram, while three MTS-100-kip actuators with a stroke length of 15 in. were used for lateral loading. Lateral loading beams were bolted to the specimens to apply the load. The axial loading was maintained constant while the cyclic lateral loading was applied. The test setup is shown in Figure 7.

Table 4. Design Calculations for Noncontact Lap Splice Connections			
Specimen	**SP-1**	**SP-2**	**SP-3**
Required Connection Strength			
$1.25A_{bar}F_{y\_bar}$, kips	33	79	33
N_r, kips	795	1885	795
Interfacial Shear Strength			
ϕR_{tie} (using Eq. 1), kips	286	714	286
ϕR_{stud} (using Eq. 2), kips	597	1493	597
$\sum_n Q_n$, kips	883	2207	883
Development Length (Wall)			
l_{d_wall} (using ACI 318-19, 25.4.2.4)*, in.	20.9	53.6	20.9
$l_{d\_wall\_provided}$, in.	22.0	55.0	22.0
Development Length (Base)			
l_{d_fnd} (using ACI 318-19, 25.4.3.1), in.	8.50	17.4	8.50
$l_{d\_fnd\_provided}$, in.	31.5	31.5	31.5
* Already multiplied by a factor of 1.3			

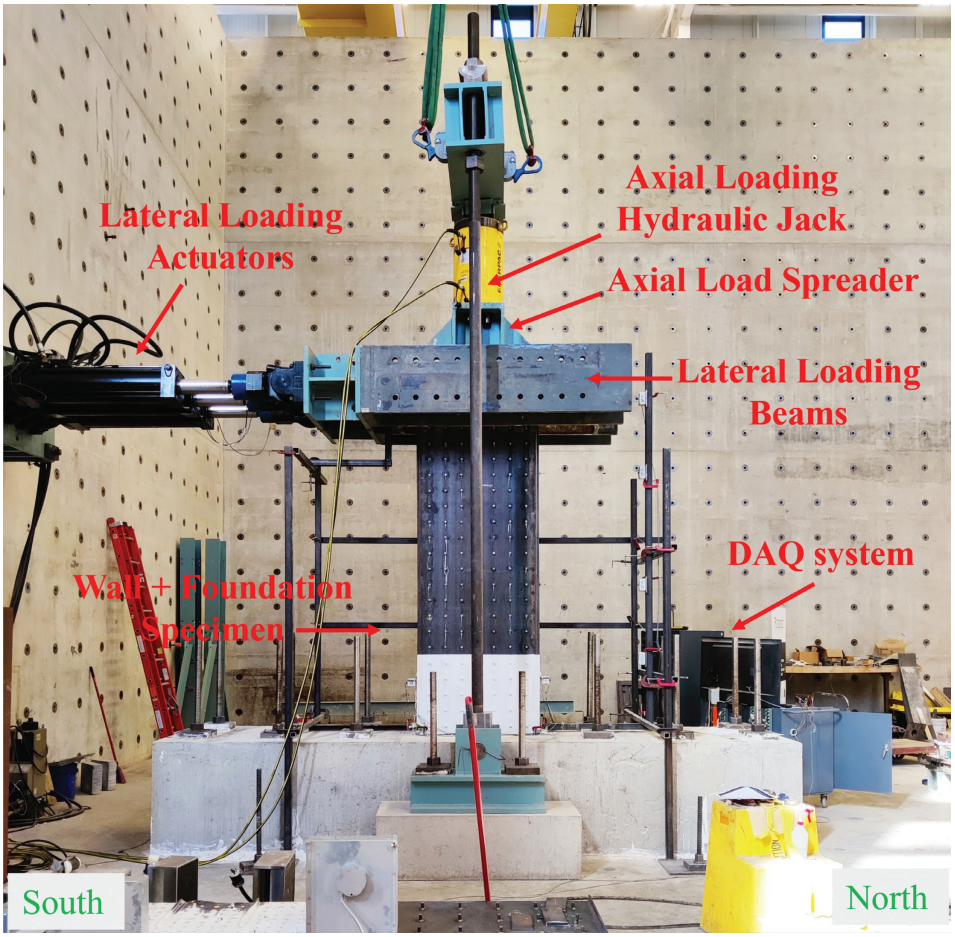

Fig. 7. View of the test setup.

Figure 8 presents the loading protocol for wind and seismic loading previously developed and used by the authors (Shafaei et al., 2021, 2023). The nominal flexural strength, M_n, used in the protocol was calculated as the nominal flexural strength of the confined RC section using the AISC *Specification* Section I-1.2a plastic stress distribution method. Nominal steel and concrete material properties were used, and the effect of axial forces was considered.

The wind loading protocol is shown in Figure 8(a). The wind loading cycles consisted of 500 force-controlled elastic cycles each at 0.25 and 0.50M_n, followed by 75 force-controlled elastic cycles at 0.75M_n. Inelastic wind cycles were applied thereafter. The yield rotation ($\theta_y = \Delta_y/h$) used for these cycles was computed based on the lateral stiffness reported in the first 0.75M_n elastic cycle. After the inelastic wind cycles, the elastic cycles were repeated to reevaluate the lateral stiffness of the specimen.

Seismic cycles in the inelastic range of behavior were performed after the wind cycles. Three cycles were applied at 2θ_y and 3θ_y, followed by two cycles at 4θ_y, 5θ_y, 6θ_y, and so on. The cycles continued until (1) a significant drop in the peak lateral loads, and base moments, was observed or (2) fracture in the specimen occurred. Figure 8(b) shows the seismic loading protocol used in experimental investigations.

Summary of Experimental Results

The experimental behavior all three specimens is summarized in this section. Despite differences in connection detailing, variations in dowel size and layout, and the inclusion of an RC wall between C-PSW/CF and RC foundation, significant similarities were observed in the overall cyclic response of SP-1, SP-2, and SP-3. Eventually, after significant inelastic cycles and ductility, tensile rupture of the dowels occurred in the confined RC section of SP-1 and SP-2, and at the RC wall-RC base interface for SP-3. This failure mode was expected as per the full-strength design approach.

Figure 9(a)–(c) present the response of the three specimens to wind and seismic loading. The applied moment at the base of the connection and the corresponding lateral

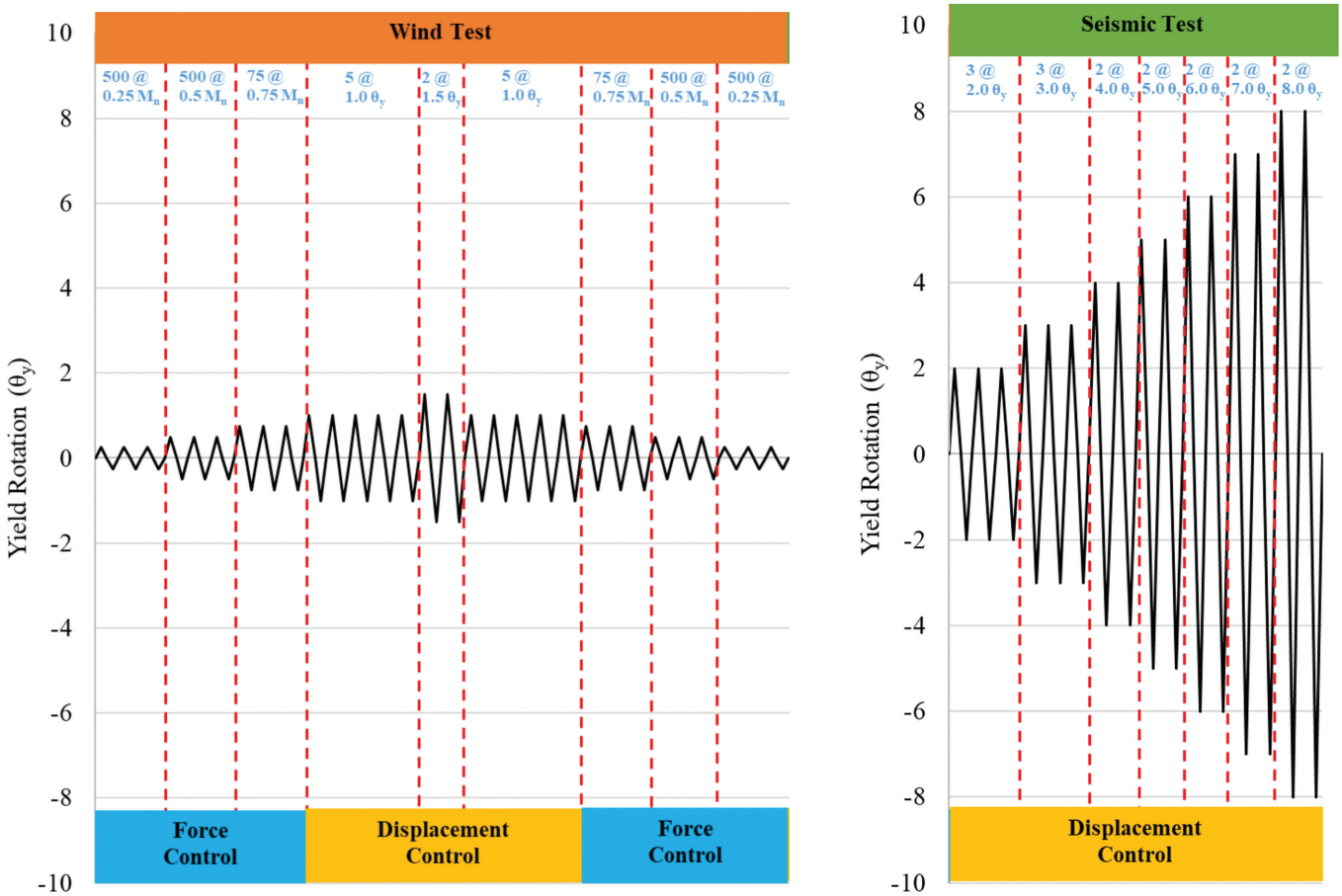

(a) Wind test *(b) Seismic test*

Fig. 8. Cyclic lateral loading protocol.

drift are shown. The lateral drift (Δ/h) is calculated by dividing the lateral displacement, Δ, at the lateral load application point by h, the distance between the load application point and the connection base. Results for all 2,162 wind cycles and seismic cycles are shown. The figure also includes horizontal dashed lines corresponding to 80% of the experimentally observed maximum capacity.

All three specimens exhibited linear behavior during the elastic wind cycles, and no major stiffness degradation was observed. Yielding of the dowels in the outermost layer was observed during the $0.75M_n$ elastic cycles across all specimens, as corroborated by the strain gauge data. Minor cracks in the RC wall were observed in SP-3 during the same cycles. Inelastic cycles at $1.0\theta_y$ and $1.5\theta_y$ led to yielding in additional dowels closer to the C-PSW/CF flanges. However, the specimens' overall behavior remained predominantly linear. During these inelastic cycles, the C-PSW/CF steel plates in SP-1 and SP-2 showed no signs of yielding, and the RC wall concrete in SP-3 remained intact. A loss in flexural stiffness was observed in the second set of elastic wind cycles, as expected.

The seismic cycles were based on the yield rotation of the specimen, θ_y, computed using the lateral stiffness reported during the first of $0.75M_n$ elastic cycle. All specimens behaved linearly during the three seismic cycles at $2\theta_y$. However, during the cycles at $3\theta_y$, minor excursions into the nonlinear range were observed. Specifically, the C-PSW/CF flanges of SP-2 exhibited yielding. In the $4\theta_y$ cycles, the C-PSW/CF flanges of SP-1 experienced yielding, while SP-2 had a loss in stiffness due to local deformations in the north C-PSW/CF flange, located between the C-PSW/CF base and the first row of flange shear studs. For SP-3, the behavior was marginally inelastic, and some cracking in the RC wall was observed. The second cycle at $5\theta_y$ resulted in a decrease in base moment and flexural stiffness for SP-2 accompanied by local deformations in the

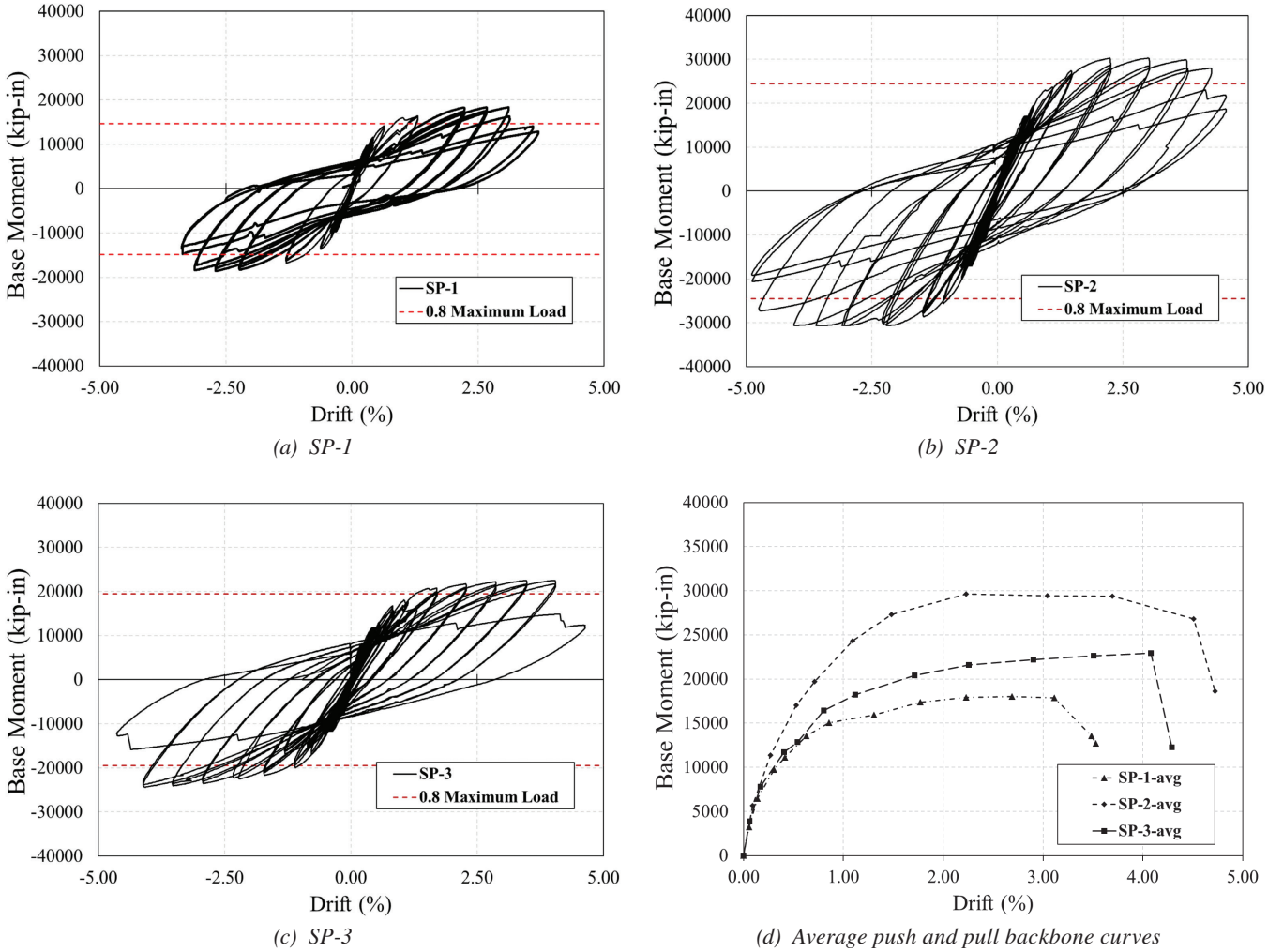

(a) SP-1 *(b) SP-2*

(c) SP-3 *(d) Average push and pull backbone curves*

Fig. 9. Base moment-drift responses.

Table 5. Measured Material Properties			
	Dowel Rebar		Concrete
Specimen	F_y (ksi)	F_u (ksi)	f'_{cm} (psi)
SP-1	66	108	7564
SP-2	91	118	7441
SP-3	69	108	8926

south C-PSW/CF flange. The south and north directions of the specimens are indicated in Figure 7. SP-1 and SP-3 also showed nonlinear behavior; however, no reduction in base moment was observed.

In $6\theta_y$ cycles, five out of six outermost dowels of SP-2 underwent tensile rupture, causing an abrupt reduction in stiffness. In addition, the maximum base moment decreased by more than 20%. An additional cycle at the same amplitude led to tensile rupture of the remaining dowel and a 40% reduction in the maximum base moment. The test was stopped as a result. SP-1 and SP-3 remained inelastic in these cycles and were subjected to two seismic cycles at $7\theta_y$. Excessive deformations in C-PSW/CF flanges of SP-1 were observed in the first cycle, while tensile rupture in one outermost dowel was observed during the second cycle. Moreover, there was a notable decrease in the maximum base moment during the second cycle. SP-3 also exhibited a highly nonlinear base moment-drift response with unchanged maximum base moments and loss in RC wall concrete cover due to cracking. However, no rupture in dowels occurred.

Both SP-1 and SP-3 were subjected to seismic cycles at $8\theta_y$. In SP-1, a decrease in the maximum base moments was seen along with tensile rupture in five outermost dowels throughout the two cycles. SP-3 was only subjected to a single cycle at $8\theta_y$, during which tensile rupture in six outermost dowels occurred. The maximum base moments in both push and pull directions reduced by more than 40%, and the test was concluded.

Figure 9(d) shows the backbone of the base moment-drift curves for the specimens. These backbone curves represent the average of the push and pull responses for the specimens. The initial behavior prior to concrete cracking is consistent for all three specimens, and no significant difference in secant stiffness is observed. However, after concrete cracking, the response of SP-2 is stiffer compared to SP-1 and SP-3 due to the presence of higher strength dowel bars. Significant changes in the base moment-drift response are observed during the seismic cycles, with losses in lateral stiffnesses because of dowel yielding. The peak base moment is highest for SP-2, due to higher strength rebar, followed by SP-3, having a larger confined RC section, and lowest for SP-1. All three specimens exhibited significant ductility prior to failure, which occurred during the $8\theta_y$ cycles for SP-1 and SP-3 and the $6\theta_y$ cycles for SP-2.

Failure in all three specimens occurred due to tensile rupture in the dowel bars. These dowels were in the peripheral (end) layers of the confined RC section. The failure occurred at the base of the C-PSW/CF for SP-1 and SP-2 and at the base of RC wall for SP-3. Following the cyclic test, concrete surrounding the ruptured dowels was removed from the specimens. Figure 10 shows the ruptured dowels on the north and south side of the specimens, with tensile failure clearly visible. The remaining dowels show no signs of failure.

FIBER-BASED MODEL OF CONFINED RC SECTION

A fiber-based model of the confined RC section in the noncontact lap splice connection region was developed and used to compute the moment curvature, M-ϕ, response. This fiber-based approach extended the Euler-Bernoulli beam bending theory, which assumes that plane sections remain plane and perpendicular to the neutral axis before and after bending. Additional assumptions included linear distribution of longitudinal strains through the cross section, full strain compatibility between the steel dowels and the surrounding concrete, and negligible tensile stress contribution from the concrete infill.

Axial loads acting on the section were considered while obtaining the M-ϕ relationship. The steel stress-strain behavior was modeled with linear elastic behavior up to the measured yield stress, F_y, followed by yield plateau, and then power-law strain hardening up to the measured ultimate stress, F_u. The concrete was modeled with stress-strain behavior based on Tao et al. (2013) up to the measured concrete strength, f'_{cm}, and plastic (no degradation in strength) behavior thereafter to account for the confinement from C-PSW/CF steel plates. The calculated M-ϕ relationship was used to evaluate the flexural stiffness and strength of the connection region, as discussed later. Table 5 includes the measured material properties used in the fiber analysis.

(a) SP-1 north side

(b) SP-1 south side

(c) SP-2 north side

(d) SP-2 south side

(e) SP-3 north side

(f) SP-3 south side

Fig. 10. Ruptured dowel bars on the north and south sides of the wall specimens.

These included the yield and tensile strengths of the dowel bars and the concrete compressive strengths.

FLEXURAL STIFFNESS

The flexural stiffness of the noncontact lap splice connection region can influence serviceability design (e.g., drift requirements). In this section, the flexural stiffness of the wall specimen, including the connection region, is estimated using experimental results and used to evaluate assumptions regarding the stiffness of the connection region. The experimental flexural stiffness, EI_{exp}, is calculated using the secant stiffness from the lateral force-displacement, H-Δ, response of the wall specimen during the $0.50M_n$ wind cycles because they are most representative of serviceability (story drift during wind cycles) performance. The specimen is assumed to be a fixed-base cantilever, and the entire specimen height is assumed to have the same effective stiffness, EI_{exp}, that can then be calculated using Equation 3. In this equation, h is the height of the wall between the fix base and lateral load location, and $(H/\Delta)_{0.50Mn}$ is the secant stiffness. Table 5 reports the experimental flexural stiffness values, EI_{exp}, for Specimens SP-1, SP-2, and SP-3.

$$EI_{exp} = \frac{h^3}{3}\left(\frac{H}{\Delta}\right)_{0.50M_n} \quad (3)$$

$$EI_{C\text{-}PSW/CF} = E_S I_S + 0.35E_c I_c \quad (4)$$

$$EI_{RC\_wall} = 0.35E_c I_g \quad (5)$$

Assumptions regarding the flexural stiffness of the connection region, EI_{con}, were then evaluated using elastic models of the specimens shown schematically in Figure 11. The composite wall portions were modeled using the flexural stiffness recommendation from AISC *Specification* Section I1.5(e) as shown in Equation 4. In this equation, $EI_{C\text{-}PSW/CF}$ is the flexural stiffness of the composite wall portion; E_s and E_c are the elastic modulus of steel and concrete, respectively; and I_s and I_c are the moments of inertia of the steel module and concrete infill of the composite cross section, respectively. The RC wall portion of Specimen SP-3 was modeled using flexural stiffness recommendations from ACI 318-19, Table 6.6.3.1.1(a), as shown in Equation 5. In this equation, EI_{RC_wall} is the flexural stiffness of the reinforced concrete wall portion of SP-3, E_c is the elastic modulus of concrete, and I_g is the moment of inertia of the gross concrete section.

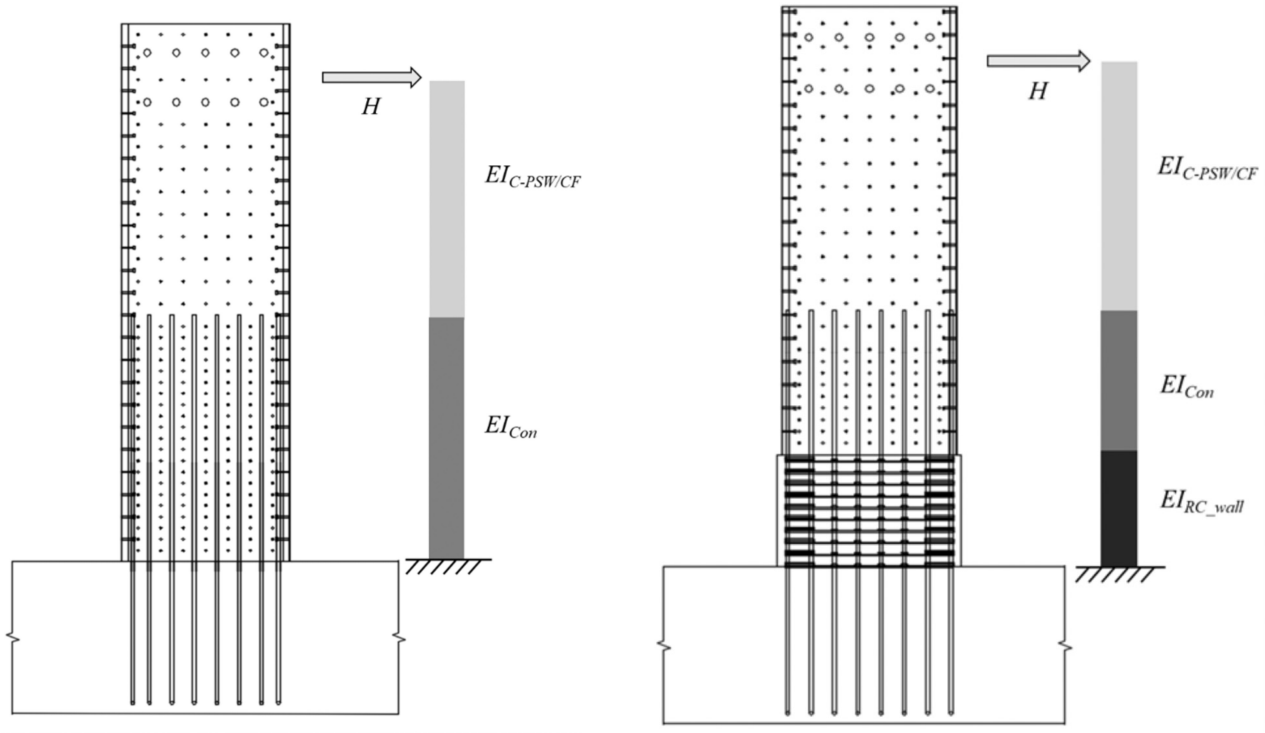

(a) SP-1 and SP-2 *(b) SP-3*

Fig. 11. Spring model system schematic.

Table 6. Flexural Stiffness Comparison (Experimental-to-Calculated)				
Specimen	**Flexural Stiffness**	**Stiffness Ratios (Experimental-to-Calculated)**		
	EI_{exp} $\times 10_6$ (kip-in.^{2})	$EI_{con} = 0.35E_cI_g$	$EI_{con} = E_sI_s + 0.35E_cI_c$	EI_{con} using M-ϕ
		$EI_{exp}/EI_{eff\text{-}i}$	$EI_{exp}/EI_{eff\text{-}ii}$	$EI_{exp}/EI_{eff\text{-}iii}$
SP-1	142	1.48	0.95	1.00
SP-2	128	1.73	1.16	0.91
SP-3	162	1.33	1.22	1.18

The connection region of the wall specimen was modeled considering three options for EI_{con}: (i) assuming that the connection region can be modeled with the same flexural stiffness as an RC wall ($EI_{con} = 0.35E_cI_g$), (ii) assuming that the connection region can be modeled with the same flexural stiffness as the composite wall ($EI_{con} = E_sI_s + 0.35E_cI_{c)}$, and (iii) assuming that the connection region flexural stiffness can be represented with the M-ϕ relationship obtained from fiber analysis of the confined RC section.

An elastic model of the specimen length with a fixed base was developed using different stiffnesses for different portions as explained above and shown schematically in Figure 11. This model was analyzed for the applied lateral loading, H, corresponding to the $0.50M_n$ cycles, and the lateral deflection, Δ, was calculated by integrating curvatures corresponding to the moments and section flexural stiffness along the height as per Lai et al. (2016). The calculated lateral deflection was used to estimate the effective (or smeared) wall stiffness using the right side of Equation 3. The estimated wall stiffnesses are referred to as $EI_{eff\text{-}i}$, $EI_{eff\text{-}ii}$, and $EI_{eff\text{-}iii}$, respectively, corresponding to the use of assumptions (i), (ii), and (iii) for the connection region stiffness.

Table 6 includes comparisons of the experimental stiffness, EI_{exp}, with the stiffness calculated using assumptions (i), (ii), and (iii) for the connection region. As shown by the ratios in the table, using assumption (i) significantly underestimates (ratios ranging from 1.33–1.73) the flexural stiffness of the walls with connection regions. Using assumption (ii) reasonably estimates the flexural stiffness (ratios ranging from 0.95–1.22) of walls with connection regions. Using assumption (iii) also reasonably estimates (ratios ranging from 0.91–1.18) the flexural stiffness of walls SP-1, SP-2, and SP-3. Due to its simplicity, assumption (ii), which models the noncontact lap splice connection region with the same flexural stiffness ($EI_{con} = E_sI_s + 0.35E_cI_c$) as the composite wall is recommended.

FLEXURAL STRENGTH

The flexural strength of the confined RC section in the connection region was calculated using analytical approaches based on ACI 318-19 code recommendations, the 2022 AISC *Specification*, and the fiber-based analysis of the cross section as mentioned earlier. These approaches inherently assume that the connection is designed and detailed appropriately with (1) sufficient interfacial shear strength, (2) adequate embedment (development) length for the dowels, and (3) appropriate placement of the dowels for a ductile failure mode. All the approaches accounted for the effects of axial force on the flexural strength and used the measured material properties for steel and concrete (reported in Table 5) in the calculations.

The ACI 318-19 approach used recommendations from Section 22.2 to compute the flexural strength. These included an extreme concrete compression fiber strain of 0.003, rectangular concrete stress distribution in compression, zero concrete stress contribution in tension, and elastic-perfectly plastic behavior for the dowels. Figure 12(a) illustrates a characteristic stress distribution in the confined RC section per ACI 318-19. In this figure, x_i is the distance from the rebar to the extreme compression fiber, and a is the depth of the rectangular (Whitney) stress block. The rebar stresses, F_i, increase linearly (in compression and tension) from the neutral axis but are limited to the maximum yield stress of F_y.

The AISC *Specification* approach used the plastic stress distribution method from *Specification* Section I1.2a to compute the flexural strength. Figure 12(b) illustrates the assumed plastic stress distribution. In this figure, a is the depth of the plastic neutral axis. The concrete in compression was assumed to reach $0.85f'_{cm}$, and its stress contribution in tension was neglected. All dowels were assumed to reach their yield strength of F_y in tension and in compression. Because the experiments eventually failed with tensile rupture of the dowels, the AISC *Specification* Section I1.2a approach was modified to assume that all dowels reach their ultimate tensile strength, F_u, and the flexural strength was calculated again.

Table 7 includes the experimental flexural strength, M_{exp}, from the tests. It also includes ratios of the experimental-to-calculated flexural strength using the approaches mentioned previously. As shown, using the ACI 318-19 method results in experimental-to-calculated strength ratios that are very

Table 7. Flexural Strength Comparisons (Experimental-to-Calculated)					
	Experimental Flexural Strength	Connection Flexural Strength Ratios (Experimental-to-Calculated)			
Specimen	M_{exp} (kip-ft)	ACI 318-19	AISC *Specification* (using F_y)	AISC *Specification* (using F_u)	M-ϕ
SP-1	1539	1.52	1.35	1.00	1.04
SP-2	2538	1.49	1.23	1.01	1.01
SP-3	1949	1.54	1.33	1.03	1.09

conservative (ratios ranging from 1.49–1.54). Using the AISC *Specification* method with yield stress, F_y, for the dowels also results in conservative experimental-to-calculated strength ratios (ranging from 1.23–1.35). However, using the AISC *Specification* method with ultimate stress, F_u, for the dowels results in accurate experimental-to-calculated strength ratios (ranging from 1.00–1.03). Similarly, using the fiber-based method also results in experimental-to-calculated strength ratios that are quite reasonable (ranging from 1.01–1.09).

Thus, the ACI 318-19 and AISC *Specification* (with F_y) approaches can be used to conservatively estimate the flexural strength of the confined RC section, and thus the connection region. Both these methods provide a lower-bound estimate of the flexural strength, but the ACI method is more conservative because it does not assume full plastification of the cross section. We recommend using the AISC *Specification* (with F_y) approach to estimate the flexural strength for design. The AISC *Specification* modified approach (using F_u instead of F_y) can be used to estimate the expected flexural strength of the confined RC section and thus the connection region. Similarly, the fiber-based analysis of the confined RC section can also be used to estimate the expected flexural strength.

SHEAR STRENGTH

The connection region is also designed with adequate shear strength to resist the corresponding (shear) demands associated with lateral loading on the C-PSW/CF wall. These shear demands are also resisted by the dowels located closer to the center (or neutral axis) of the confined RC section. The dowels resist the shear demands in direct shear, which is indicated by their deformed shapes at the end of testing and observed after removal of concrete (Varma et al., 2024).

For a lap splice connection with dowels having a gross cross-sectional area of A_{bar} and nominal yield strength of F_{y_bar}, the shear strength can be calculated as the direct shear strength ($0.6A_{bar}F_{y\_bar}$) of approximately 80% of the rebar in the connection, resulting in an estimated shear strength of $0.5A_{bar}F_{y\_bar}$. The ratio of the maximum lateral load (or base shear) from the experiment, H_{exp}, and the

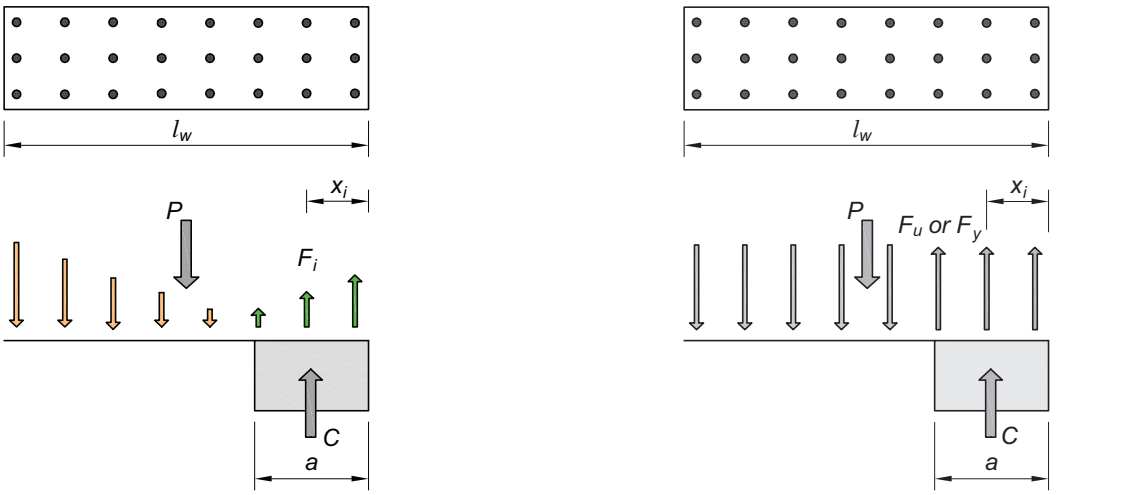

(a) ACI 318 approach *(b) AISC* Specification *plastic distribution approach*

Fig. 12. Analytical approaches for flexural strength calculation.

Table 8. Shear Demand to Estimated Strength Ratios		
	Maximum Lateral Load (kips)	Shear Strength Ratios (Experimental-to-Calculated)
Specimen	H_{exp}	$H_{exp}/0.5A_{bar}F_y$
SP-1	171	0.49
SP-2	282	0.33
SP-3	217	0.60

calculated expected shear strength, $0.5A_{bar}F_y$, for the tested specimens is provided in Table 8. As shown, the shear demand was just a fraction of the calculated shear strength with experimental-to-calculated strength ratios ranging from 0.33 to 0.60. This agrees with experimental results where no shear failure or cracking was observed.

The ratios of H_{exp} with respect to the upper limit of shear strength for reinforced concrete walls from ACI 318-19, Section 18.10.4.1 (mentioned earlier), were equal to 0.53, 0.87, and 0.49 for Specimens SP-1, SP-2, and SP-3, respectively. These ratios were calculated using measured material strengths and are provided for informational purposes and do not have any direct implication on the design of the confined RC section in the connection region.

CONCLUSIONS

This paper provides information on the design and detailing of noncontact lap splice connections for C-PSW/CF to RC base. These connections may be used to directly connect the C-PSW/CF to the RC foundation, or to an intermediate RC wall. They were designed to develop the full strength of the weaker of the connected parts, which is typically associated with 1.25 times the nominal yield strength of the dowels in the connection. Accordingly, previous design considerations proposed for noncontact lap splice connections for SC walls were applied here for C-PSW/CF-RC base connections. These primarily included (1) dowel development length, (2) interfacial shear strength, and (3) dowel layout.

Experimental investigations were conducted on large-scale C-PSW/CF-to-RC base specimens, and their response under wind and seismic loading was evaluated. Experimental results indicated that appropriately designed and detailed connections have excellent performance (stiffness, strength, and ductility), which are primarily governed by the behavior of the "confined RC section" in the connection region. Methods to estimate the flexural stiffness and flexural strength of the confined RC were evaluated. The following conclusions are drawn from the investigations:

1. The design recommendations offered by Seo and Varma (2017) and Seo et al. (2021) are effective and could be applied to detail C-PSW/CF-to-RC base connections. Specimens that were designed and detailed using these recommendations developed the full strength of confined RC section in the connection region as intended for ductile failure modes.
2. The specimens were able to resist wind cycles without any significant loss in lateral stiffness or yielding in the C-PSW/CF steel plates. However, minor yielding in the dowels was observed during the $0.75M_n$ cycles. In the seismic cycles, a reduction in the lateral stiffness of the specimens was apparent after excursions into the inelastic range of the behavior.
3. The seismic response of the specimens was very ductile, with SP-1, SP-2, and SP-3 failing during $8\theta_y$, $6\theta_y$, and $8\theta_y$ cycles, respectively, due to tensile rupture of multiple dowel bars. This can be attributed to the confinement provided by the steel plates of the C-PSW/CF to the concrete infill, inhibiting concrete spalling and delaying the buckling of the dowel.
4. Modeling the connection region with the same flexural stiffness as an RC wall ($EI_{con} = 0.35E_cI_g$) significantly underestimates the stiffness of walls with connection regions. Modeling the connection region with the same flexural stiffness as the composite wall ($EI_{con} = 0.35E_cI_c + E_sI_s$) adequately represents the stiffness of walls with connection regions.
5. Modeling the connection region using the moment-curvature relationship (M-ϕ) obtained from fiber analysis of the confined RC section also adequately represents the stiffness of walls with connection regions. However, due to its simplicity, modeling the connection regions with the same flexural stiffness as the composite wall is recommended.
6. The design flexural strength of the confined RC section in the connection region can be calculated conservatively using the AISC *Specification* Section I1.2a plastic stress distribution method. Calculating this flexural strength using ACI 318-19 code recommendations can be too conservative.
7. The expected flexural strength of the confined RC section in the connection region can be calculated accurately by

modifying the AISC *Specification* Section I1.2a plastic stress distribution method to use the ultimate or tensile stress, F_u, for the dowels instead of the yield stress, F_y. This expected flexural strength can also be estimated with reasonable accuracy using the fiber-based section moment-curvature (M-ϕ) analysis method.

8. Overall, noncontact lap splice connections are an effective method to connect C-PSW/CF walls to RC bases. They can be detailed and designed appropriately to achieve the full strength of the confined RC section in the connection region resulting in excellent stiffness, strength, and ductility of the composite wall system.

ACKNOWLEDGMENTS

The project was supported by Charles Pankow Foundation (CPF Research Grant 06–16) and the American Institute of Steel Construction (AISC). However, any opinions, findings, conclusions, and recommendations presented in this paper are those of the authors and do not necessarily reflect the view of the sponsors.

SYMBOLS

The following symbols are used in this paper:

A_{bar}	Gross cross-sectional area of dowel bars in the connection
A_{cv}	Cross-sectional area of concrete in confined RC section
A_{tie}	Area of tie bar
A_{stud}	Area of tie bar
E_c	Modulus of elasticity of concrete
EI_{exp}	Experimental flexural stiffness
EI_{con}	Flexural stiffness of the connection region
$EI_{C\text{-}PSW/CF}$	Flexural stiffness of the C-PSW/CF portion
EI_{RC_wall}	Flexural stiffness of the RC wall portion
E_s	Modulus of elasticity of steel
F_y	Measured dowel bar yield strength
F_{y_bar}	Dowel bar nominal yield strength
F_{y_tie}	Tie bar/threaded rod nominal yield strength
F_u	Measured dowel bar ultimate strength
F_{u_stud}	Stud anchor (shear stud) nominal ultimate strength
H	Lateral load applied at level of loading actuators
H_n	Lateral force corresponding to the nominal flexural strength of the confined RC section
H_{exp}	Maximum experimental lateral load
I_c	Moment of inertia of C-PSW/CF infill concrete core
I_g	Moment of inertia of RC wall section
I_s	Moment of inertia of C-PSW/CF steel section
M_{exp}	Maximum experimental moment strength
M_n	Nominal flexural strength of the confined RC section
N_r	Required tensile strength
Q_n	Shear resistance of individual anchor/tie bar
R_{stud}	Direct shear strength of the stud anchor
R_{tie}	Direct shear strength of the tie bar/threaded rods
S	Smallest distance between rows of tie bars or shear studs
d_{bar}	Diameter of dowel bar
d_{stud}	Diameter of shear stud
d_{tie}	Diameter of tie bar
f'_c	Nominal concrete compression strength
f'_{cm}	Measured concrete compression strength
h	Distance between the load application point and the connection base
h_w	Wall height
l_{d_fnd}	Dowel bar foundation development length
$l_{d\_fnd\_provided}$	Provided dowel bar foundation development length
l_{d_wall}	Dowel bar wall development length
$l_{d\_wall\_provided}$	Provided dowel bar wall development length
l_w	C-PSW/CF wall length
s_{stud}	Shear stud spacing
s_{tie}	Tie bar spacing
t_p	C-PSW/CF steel plate thickness
t_{sc}	C-PSW/CF wall thickness
t_w	RC wall thickness
α_c	Coefficient of concrete contribution to wall shear strength

Δ	Lateral displacement
Δ_y	Yield displacement
ρ	Steel reinforcement ratio
ρ_l	Longitudinal wall reinforcement ratio
ρ_t	Transverse wall reinforcement ratio
ρ_{tie}	Tie bar reinforcement ratio
θ_y	Yield rotation

REFERENCES

ACI (2019), *Building Code Requirements for Structural Concrete and Commentary*, ACI 318-19, American Concrete Institute, Farmington Hills, Mich.

Agrawal, S., Broberg, M., and Varma, A.H. (2020), "Seismic Design Coefficients for SpeedCore or Composite Plate Shear Walls-Concrete Filled (C-PSW/CF)," Bowen Laboratory Research Report, Purdue University, West Lafayette, Ind.

Ahmad, M,. Shafaei, S., Varma, A.H., and Klemencic, R. (2024), "Experimental Investigation of Composite Coupling Beam-to-Wall Connections in Coupled C-PSW/CF Systems." *Journal of Structural Engineering*, ASCE Vol. 150, No. 9, 04024114. https://doi.org/10.1061/JSENDH.STENG-13453

AISC (2016), *Seismic Provisions for Structural Steel Buildings*, ANSI/AISC 341-16, American Institute of Steel Construction, Chicago, Ill.

AISC (2022a), *Seismic Provisions for Structural Steel Buildings,* ANSI/AISC 341-22, American Institute of Steel Construction, Chicago, Ill.

AISC (2022b), *Specification for Structural Steel Buildings*, ANSI/AISC 360-22, American Institute of Steel Construction, Chicago, Ill.

AISC (2024), "*Specification for Safety-Related Steel Structures for Nuclear Facilities*, ANSI/AISC N690-24, American Institute of Steel Construction, Chicago, Ill.

ASCE (2016), *Minimum Design Loads for Buildings and Other Structures*, ASCE 7-16, American Society of Civil Engineers, Reston, Va.

ASCE (2022), *Minimum Design Loads for Buildings and Other Structures*, ASCE 7-22, American Society of Civil Engineers, Reston, Va.

ASTM (2021), *Standard Specification for High-Strength Low-Alloy Columbium-Vanadium Structural Steel,* ASTM A572/A572M, American Society for Testing and Materials, West Conshohocken, Pa.

ASTM (2023), *Standard Specification for Alloy-Steel and Stainless Steel Bolting for High Temperature or High Pressure Service and Other Special Purpose Applications,* ASTM A193/A193M, American Society for Testing and Materials, West Conshohocken, Pa.

Bhardwaj, S.R. and Varma, A.H. (2017*), Design of Modular Steel Plate Composite (SC) Walls for Safety-Related Nuclear Facilitie*s, Design Guide 32, AISC, Chicago, Ill.

Bhardwaj, S., Varma, A.H., and Malushte, S. (2017), "Minimum Requirements and Section Detailing Provisions for Steel-Plate Composite (SC) Walls in Safety-Related Nuclear Facilities," *Engineering Journal*, AISC, Vol. 54, No. 2, pp. 89–107.

Broberg, M., Agrawal, S., Varma, A., and Klemencic, R. (2023), "Seismic Design Parameters (R, Wo, and Cd) for Uncoupled Composite Plate Shear Walls–Concrete Filled," *Earthquake Engineering and Structural Dynamics*, Vol. 52, No. 10, pp. 3,149–3,170. https://doi.org/10.1002/eqe.3917

Broberg, M., Shafaei, S., Kizilarslan, E., Seo, J., Varma, A.H., Bruneau, M., and Klemencic, R. (2022), "Capacity Design of Coupled Composite Plate Shear Walls/Concrete Filled (CC-PSW/CF)," *Journal of Structural Engineering*, ASCE, Vol. 148, No. 4. https://dx.doi.org/10.1061/(ASCE)ST.1943–541X.0003296

Kizilarslan, E., Broberg, M., Shafaei, S., Varma, A.H., and Bruenau, M. (2021), "Seismic Design Coefficients and Factors for Coupled Composite Plate Shear Walls/Concrete Filled (CC-PSW/CF)," *Engineering Structures*, Elsevier, Vol. 244, 112766. https://doi.org/10.1016/j.engstruct.2021.112766

Klemencic, R., Kraning, C., Wend, C., Englund, K., Grimmer, C., and Mills, M. (2023), "200 Park Avenue—SpeedCore 2.0 from Three Perspectives," *Structures Magazine*, ASCE.

Kurt, E.G., Seo, J., and Varma, A.H. (2022), "SC Wall-to-RC Basemat Over-Strength Connection: Behavior and Design*," Civil Engineering*, Vol. 3, No. 2, pp. 503–524. https://doi.org/10.3390/civileng3020030

Lai, Z., Varma, A.H., and Connor, R.J. (2016), "Retrofit of Built-Up Steel Columns: Modeling and Fundamental Behavior," *Journal of Bridge Engineering,* ASCE, Vol. 21, No. 3. http://dx.doi.org/10.1061/(ASCE)BE.1943–5592.0000808

Seo, J. and Varma, A.H., (2017). "Experimental Behavior and Design of Steel Plate Composite-to-Reinforced Concrete (SC-to-RC) Lap Splice Connections," *Journal of Structural Engineering*, ASCE Vol. 143, No. 5. http://dx.doi.org/10.1061/(ASCE)ST.1943–541X.0001711

Seo, J., Varma, A.H., and Zhang, K. (2019), "Pushout Behavior of SC Wall Shear Connector," *Transactions,* SMiRT-25, Charlotte, N.C., August 4–19, 10 pp., IASMIRT. https://www.lib.ncsu.edu/resolver/1840.20/37769

Seo, J., Varma, A.H., and Zhang, K. (2021), "Non-Contact Lap Splice Connections of Steel-Plate Composite Wall-to-Reinforced Concrete Structures," *Engineering Structures*, Elsevier, Vol. 246, 112954. https://doi.org/10.1016/j.engstruct.2021.112954

Shafaei, S., Varma, A., Huber, D., and Klemencic, R., (2023), "Lateral Load Behavior of C-PSW/CFs Using Steel Members as Boundary Elements," *Journal of Structural Engineering*, ASCE, Vol. 149, No. 9, 04023112. https://doi.org/10.1061/JSENDH.STENG-12085

Shafaei, S., Varma, A.H., and Klemencic, R. (2021), "Cyclic Lateral Loading Behavior of Composite Plate Shear Walls/Concrete Filled (C-PSW/CF)," *Journal of Structural Engineering*, ASCE, Vol. 147, No. 10. https://doi.org/10.1061/(ASCE)ST.1943–541X.0003091

Shafaei, S., Varma, A.H., Seo, J., Huber, D., and Klemencic, R. (2022), "Wind Design of Composite Plate Shear Walls/Concrete Filled (SpeedCore) Systems," *Engineering Journal*, AISC, Vol. 59, No. 3, pp. 183–208.

Tao, Z., Wang, Z., and Yu, Q. (2013), "Finite Element Modelling of Concrete-Filled Steel Stub Columns under Axial Compression," *Journal of Construction Steel Research,* Elsevier, Vol. 89, pp. 121–131. https://doi:10.1016/j.jcsr.2013.07.001

Traut-Todaro, J. (2019), "SpeedCore, Lateral System Innovation for Today's Construction Challenges," *Modern Steel Construction,* AISC, November.

Varma, A.H., Broberg, M., Shafaei, S., and Anvari, A. (2023), *SpeedCore Systems for Steel Structures,* Design Guide 38, AISC, Chicago, Ill.

Varma, A.H., Shafaei, S., and Sharma, S. (2024), "Wind and Seismic Behavior and Design of C-PSW/CF-to-RC Foundation or Wall Connections," Final Report (CPF Research Grant 06–16), Charles Pankow Foundation, Haymarket, Va.

Wang, N., Zhou, F., Xu, H., and Xu, Z. (2020), "Experimental Study on Steel-Plate Composite Wall-to-Foundation Connections Subjected to Combined Axial Compression and Cyclic Lateral-Force," *Engineering Structures,* Elsevier, Vol. 207, 110205. https://doi.org/10.1016/j.engstruct.2020.110205